Generalized Predictive Control of Temperature on an Atomic Layer Deposition Reactor

Wen-Jie He, *Student Member, IEEE*, Hai-Tao Zhang, *Senior Member, IEEE*, Zhiyong Chen, *Senior Member, IEEE*, Bo Chu, Kun Cao, Bin Shan, and Rong Chen, *Member, IEEE*

***Abstract*— This brief establishes a closed-loop control system for a radiant heating atomic layer deposition (ALD) reactor using generalized predictive control (GPC). The GPC-based closed-loop control system can rapidly and precisely stabilize the temperature in the presence of external disturbances. Compared with the conventional open-loop control and the proportional–integral–differential control, the closed-loop GPC system enhances the processing efficiency between every ALD run by substantially reducing settling time with impact by external disturbances. The attenuated temperature fluctuation leads to more uniform thin-film morphologies that fulfill the technical requirements of ALD processes.**

***Index Terms*— Atomic layer deposition (ALD), external disturbance, nanometer thin film, predictive control, temperature control.**

I. Introduction

ATOMIC layer deposition (ALD) is a powerful thin-film deposition technique that uses sequential self-terminating surface reactions to achieve subnanometer scale control of growth processes [1]–[3]. The surface-reaction-controlled deposition mechanism ensures precise control of film thickness, conformality, and uniformity over large areas [4]. Therefore, ALD has recently attracted increasing attention for its application in microelectronics, environmental protection, and renewable energy [5]–[7].

Temperature is one of the two dominant conditions that affect ALD process quality and efficiency (the other being partial pressure). However, the allowable operating temperature range for ALD reactions is narrow, thus substrate temperature must be quickly and precisely stabilized at the set point to prevent undesired side reactions, such as precursor condensation, reactant decomposition, gas phase reevaporation, and vapor phase side reactions [8]. Furthermore, precise and efficient control of the chamber temperature is crucial to guarantee uniformity of film thickness and conformality during sequential ALD runs. However, it is challenging to design an effective controller for ALD that accounts for three major types of external disturbances: 1) chamber pressure variation; 2) precursor pulse; and 3) sample manipulation between consecutive runs. This brief seeks to develop a temperature control system that substantially improves both production efficiency and quality of ALD processes that are impacted by complicated external disturbances.

In most of the existing ALD reactors, the temperature is controlled by proportional–integral–differential (PID) strategy, which is easy to set up. But because PID is a linear control method while ALD temperature follows a nonlinear dynamics within operation ranges, PID could not provide a satisfactory control performance for the whole ALD process. Moreover, ALD processes are always suffered by long time delay (due to the radiation heating manner), external noises, and uncertainties, which even increase the difficulty of PID tuning. Hence, the settling time is not sufficiently short and the overshoot is large, which often leads to precursor decomposition. Thus, we have to seek assistance from a more suitable advanced control strategy, which has nice adaptivity and capability to deal with the nonlinear thermal dynamics and external disturbances of the ALD chamber.

Model predictive control (MPC) is recognized as an effective control method for many industrial process applications, especially in chemical processes and power systems [9]–[15]. Generalized predictive control (GPC) is a special case of MPC, and has shown its superiority in controlling reactor temperatures [16]–[18]. GPC uses receding horizon optimization and output rectification that provide robustness to external disturbances and uncertainties [19]–[21]. Specifically, when compared with general MPC methods with internal state-space models, GPC adopts the controlled autoregressive integrated moving average (CARIMA) model [19], which can be efficiently identified and tuned online by sampling input–output data.

Manuscript received January 18, 2015; revised February 3, 2015; accepted February 7, 2015. Manuscript received in final form February 8, 2015. This work was supported in part by the National Basic Research Program of China under Grant 2013CB934800, in part by the National Natural Science Foundation of China under Grant 51101064, Grant 61322304, Grant 51120155001, and Grant 51328501, in part by the Thousand Young Talents Plan, in part by the Recruitment Program of Global Experts, in part by the Fundamental Research Funds for the Central Universities through the Huazhong University of Science and Technology, Wuhan, China, under Grant 2014TS037, in part by the Program for Changjiang Scholars and Innovative Research Team in University under Grant IRT13017, and in part by the Specialized Research Fund for the Doctoral Program of Higher Education with Grant No. 20130142110050. Recommended by Associate Editor F. A. Cuzzola. *(Corresponding authors: R. Chen and H. T. Zhang.)*

W.-J. He, B. Chu, and R. Chen are with the State Key Laboratory of Digital Manufacturing Equipment and Technology, School of Mechanical Science and Engineering, Huazhong University of Science and Technology, Wuhan 430071, China (e-mail: wenjie.he101@gmail.com; chubo1060@gmail.com; rongchen@mail.hust.edu.cn).

H.-T. Zhang is with the Key Laboratory of Image Processing and Intelligent Control, School of Automation, and the State Key Laboratory of Digital Manufacturing Equipment and Technology, Huazhong University of Science and Technology, Wuhan 430071, China (e-mail: zht@mail.hust.edu.cn).

Z. Chen is with the School of Electrical Engineering and Computer Science, University of Newcastle, Callaghan, NSW 2308, Australia (e-mail: zhiyong.chen@newcastle.edu.au).

K. Cao and B. Shan are with the State Key Laboratory of Material Processing and Die and Mould Technology, School of Materials Science and Engineering, Huazhong University of Science and Technology, Wuhan 430074, China (e-mail: caokunhust@gmail.com; bshan@ mail.hust.edu.cn).

Color versions of one or more of the figures in this paper are available online at http://ieeexplore.ieee.org.

Digital Object Identifier 10.1109/TCST.2015.2404898

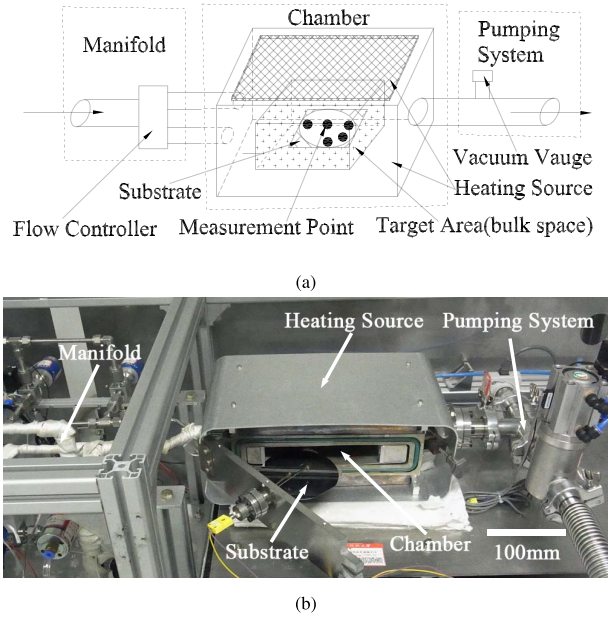

Fig. 1. Radiant heating ALD reactor. (a) Schematic. (b) Picture of the real platform.

Moreover, GPC uses the Diophantine equation of CARIMA model to derive the past and future dynamics to facilitate the predictive controller design. The GPC used in this brief does not consider hard constraints on input/output/state as they do not arise as a major issue in the present ALD process.

However, to date, there are few studies that apply MPC or other advanced control approaches to controlling temperature in ALD reactors. The reason is twofold.

1) ALD reactor chambers are generally small, and hence, it is difficult to distribute sensors and actuators in a limited space.
2) ALD requires a balance between computational efficiency and disturbance rejection capability.

Therefore, with the development of ALD technology, accurate and efficient control of chamber temperature becomes a bottleneck in improving the quality of nanosized films under the influence of external disturbances. Due to the concise internal model and capacity for dealing with external disturbances and system uncertainties, we have developed a GPC-based closed-loop control system that efficiently stabilizes temperature with precision to facilitate film growth in an ALD reactor.

This brief is organized as follows. Section II presents a description of the system along with the dynamics model. Section III develops the GPC-based closed-loop control system with a detailed control parameter optimization method. In Section IV, the robustness of GPC is studied by performing control experiments with three typical disturbances. In Section V, the improved uniformity of a deposited thin film is shown to verify the effectiveness and superiority of the developed GPC system. Finally, the conclusion is given in Section VI.

II. System Description

A radiant heating ALD reactor was built with a size of $156 \times 122 \times 26$ mm^3, as shown in Fig. 1. Compared with conductive heating, the radiant heating method has an advantage in uniformly heating both nonflat substrates and 3-D samples. The reactor consists of a gas manifold, a reaction chamber, and a pumping system. As shown in Fig. 1, the gas manifold includes Swagelok 1/4-in tubes, precursor bottles, needle valves, and mass flow controllers (MFCs) for carrier gas and purge gas. The reaction chamber has a sample holder attached to the reactor door situated between two heaters above and below the sample. The temperature of the vacuum chamber is measured by a platinum resistance needle sensor whose signal is transmitted through a power line carrier (PLC) A/D module. The pumping system consists of a vacuum gauge and a rotary vane pump. Air cooling is used to reduce the temperature in the chamber.

During an ALD run, inert gas carries precursor vapor into the reaction chamber, and the ALD growth process begins when the chamber temperature reaches the target range (100 °C–300 °C for most ALD reactions). Upon completion of the chemical adsorption process, the residual gas is purged with a continuously flowing inert carrier gas, and then pumped down by a rotary vane pump. The system pressure is determined at steady-state inert gas flow rate and pumping speed. Temperature, mass flow rate, and vacuum pressure are transmitted to a Siemens PLC series, where the PLC program communicates with a computer through a serial port and compiles data in MATLAB by an object linking and embedding for process control module.

During ALD processes, the chamber goes through four sequential stages: heating, pumping down, reaction, and venting. The heating stage occurs in preparation for the ALD process. More precisely, when the temperature reaches its target range, a sample is loaded into the chamber, and the system is pumped to a base pressure of 10 Pa during the pumping stage. The reaction stage corresponds to the film deposition process, and the venting stage prepares for the sample removal upon the completion of the ALD reaction. Different stages have different pressures, which are realized by changing the states of both the pump and the MFC, as shown in Table I.

Due to more effective air cooling at high temperatures, 150 °C is selected as the set point. According to heat transfer theory [22], a radiant heating ALD reactor can be approximately modeled by a first-order transfer function with a time delay

$$y = G(s)u, \quad G(s) = \frac{K}{Ts+1}e^{-\tau} \tag{1}$$

where the input $u(t)$ is the heater voltage, the output $y(t)$ is the chamber temperature, K is the steady-state gain, τ represents the time delay, and T denotes the time constant of the chamber. The system identifications are implemented on 3.5 V step-response data at the four different stages separately, as shown in Fig. 2. The identified model parameters are listed in Table I. The time constant is largest during the venting stage and smallest during the heating stage. This trend is caused by the weakening thermal convection effect at declining pressures in the radiant heating ALD system, and more heat is dissipated with increasing carrier gas flow rate. Considering the chamber pressure and the gas flow rate simultaneously, a time constant of 500 sccm (standard-state cubic centimeters

TABLE I
SYSTEM PARAMETERS OF FOUR STAGES

	Pump switch	Mass flow (sccm)	Pressure (P_a)	Gain K ($^\circ C$)	Time constant $T(s)$	Time delay τ (s)
1 (Heating)	close	0	101325	36.9	2417	196
2 (Pumping down)	open	0	10	34.9	2740	225
3 (Reaction)	open	100	80	35.1	2628	206
4 (Venting)	open	500	300	34.3	3163	227

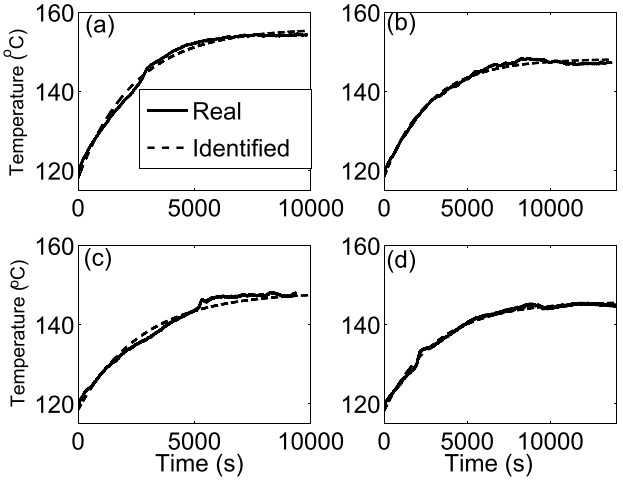

Fig. 2. Step response curves on (a) heating up, (b) pumping down, (c) reaction, and (d) venting stages.

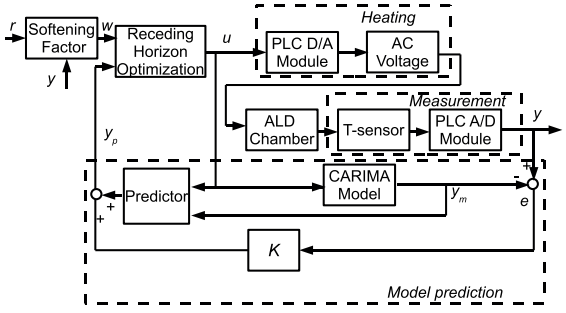

Fig. 3. Closed-loop control system structure of the radiant heating ALD reactor.

per minute) mass flow is the largest. It is worth mentioning that the identified parameters also work for other temperatures near 150 °C, since the GPC algorithm is robust for internal model mismatch [19], [23].

III. CLOSED-LOOP CONTROL SYSTEM ESTABLISHMENT

The closed-loop GPC system structure discussed in Section II is shown in Fig. 3. The control process includes three modules: 1) model prediction; 2) receding horizon optimization; and 3) feedback rectification. First, an initial actuating voltage is fed to the PLC to heat the reactor, and the temperature is monitored by a platinum resistance sensor and transmitted to the PLC and computer. In the computer, the CARIMA model is identified online and is later used to predict the evolution of chamber temperature. Meanwhile, the control input is calculated by a quadratic receding horizon optimization method. Finally, the calculated control value is fed back to the PLC-DA module to operate the heaters.

To investigate further, we briefly introduce the GPC scheme as follows [24], [25]. First, the internal CARIMA model is described as

$$A(z^{-1})y(t) = z^{-d}B(z^{-1})u(t-1) + \xi(t)/\Delta \tag{2}$$

where $t = 0, 1, \ldots$ is the discrete time constant, the symbol z^{-1} is the one-step backward operator fulfilling $z^{-1}x(t) = x(t-1)$ for any discrete time signal $x(t)$, the integer d refers to the input–output time delay, and the sampling period is 1 s. The polynomials

$$\begin{aligned} A(z^{-1}) &:= a_n z^{-n} + \cdots + a_1 z^{-1} + 1 \\ B(z^{-1}) &:= b_m z^{-m} + \cdots + b_1 z^{-1} + b_0 \end{aligned} \tag{3}$$

are obtained by the discretization of the continuous transfer function (1). Zero-mean white noise $\xi(t)$ is also added to the model through the the operator $\Delta := 1 - z^{-1}$. In particular, for any signal $x(t)$, $\Delta x(t) = x(t) - x(t-1)$ represents the signal variation.

In the framework of MPC, we use the symbol $y(t+j|t)$ to represent the predicted state y at the time $t+j$ using the information available at the time t. Using the Diophantine equation

$$\mathbf{I} = E_j(z^{-1})\Delta A(z^{-1}) + z^{-j}F_j(z^{-1}) \tag{4}$$

with a unit matix $\mathbf{I}$, the future dynamics are derived as

$$y(t+j|t) = G_j(z^{-1})\Delta u(t+j-d-1) + F_j(z^{-1})y(t) \tag{5}$$

with polynomials $E_j(z^{-1})$ and $F_j(z^{-1})$ of degree no greater than $j-1$ and $n-1$, respectively, and polynomial $G_j(z^{-1}) = E_j(z^{-1})B(z^{-1})$.

We mainly consider an optimization problem to minimize a quadratic index

$$\begin{aligned} J(t) = &\sum_{j=1}^{H_p}(y(t+j|t) - w(t+j|t))^2 \\ &+ \sum_{j=1}^{H_u}\lambda(\Delta u(t+j-1|t))^2 \end{aligned} \tag{6}$$

where H_p and H_u are the prediction and control horizons, respectively, and $\lambda > 0$ is the weighting factor. The signal $w(t+j|t)$ denotes the future reference trajectory predicted by

$$w(t+j|t) = \alpha^j y(t) + (1-\alpha^j)r(t), \quad j = 1, 2, \ldots, H_p \tag{7}$$

where $r(t)$ is the set point and $\alpha \in (0,1)$ is the softening factor to alleviate the aggressiveness of the control law [25]. The first and second terms of the index $J(t)$ penalize the future temperature tracking error and the control cost, respectively.

The optimization problem to minimize the index (6) can be solved by an analytical solution $\Delta U^*(t|t) := [\Delta u^*(t|t), \ldots, \Delta u^*(t+H_u-1|t)]^T$ that is obtained by solving $\partial J(t)/\partial U(t) = 0$ as follows:

$$\begin{aligned} \Delta U^*(t|t) = &(\mathbf{G}^T(t)\mathbf{G}(t) + \lambda \mathbf{I}_{H_u})^{-1} \\ &\cdot \mathbf{G}^T(t)(\mathbf{w}(t) - \mathbf{f}(t)). \end{aligned} \tag{8}$$

Only the first entry is extracted as the actual control variation signal, using the receding horizon approach

$$\Delta u^*(t) = \Delta u^*(t|t) = e_{H_u} \cdot \Delta U^*(t|t) \tag{9}$$

with $e_{H_u} := [1, 0, \ldots, 0]_{1\times H_u}$. As a result, the optimal control law is implemented as $u^*(t) = u^*(t-1) + \Delta u^*(t)$, which is the real voltage command transmitted to the PLC-DA module to heat the reactor.

In (8), $\mathbf{I}_{H_u}$ is an H_u-dimensional unit matrix and the vector $\mathbf{f}(t) := [f_0(t), f_1(t), \ldots, f_{H_p-1}(t)]^T$ is the predicted free response vector of the process, namely, the response if the future input trajectory remains at the most recent value $u(k-1)$. It is recursively calculated by $f_{j+1}(t) = z(1 - \Delta A(z^{-1}))f_j(t) + B(z^{-1})\Delta u(t+j-1)$ with $f_0(t) = y(t)$, $j = 0, 1, \ldots, H_p - 2$. The matrix $\mathbf{G}(t)$ is defined as

$$\mathbf{G}(t) := \begin{bmatrix} g_0(t) & \cdots & 0 \\ \vdots & \ddots & 0 \\ g_{Hu-1}(t) & \cdots & g_0(t) \\ \vdots & \vdots & \vdots \\ g_{Hp-1}(t) & \cdots & g_{Hp-Hu}(t) \end{bmatrix}_{H_p\times H_u} \tag{10}$$

with g_i representing the predicted ith step response to a unit step input $\Delta u(t) = 1(t)$. The matrix $\mathbf{G}(t)$ is calculated by the transfer function Eq. (1). The reference vector $\mathbf{w}(t) := [w(t+1|t), \ldots, w(t+H_p|t)]^T$ denotes the predicted future reference trajectory defined in (7).

The polynomials $A(z^{-1})$ and $B(z^{-1})$ in (3), i.e., $\theta := [a_1, a_2, \ldots, a_n, b_0, b_1, \ldots, b_m]^T$, are influenced by system uncertainty and external disturbances. Therefore, these parameters are identified online by recursive least squares estimation (RLSE). Let $\widehat{\theta}$ be the estimation of θ. The RLSE strategy is described as follows:

$$\begin{aligned} \widehat{\theta}(t) &= \widehat{\theta}(t-1) + K(t)[\Delta y(t) - \varphi^T(t)\widehat{\theta}(t-1)] \\ K(t) &= P(t-1)\varphi(t)[\varphi^T(t)P(t-1)\varphi(t) + \mu]^{-1} \\ P(t) &= \left(\frac{1}{\mu}\right)\left[\mathbf{I} - K(t)\varphi^T(t)\right]P(t-1) \end{aligned} \tag{11}$$

where $P(t) \in \mathbb{R}^{(m+n+1)\times(m+n+1)}$, $K(t), \varphi(t) \in \mathbb{R}^{m+n+1}$, $\mu \in (0, 1)$ is the forgetting factor, and $\varphi(t) := [-\Delta y(t-1), \ldots, -\Delta y(t-n), \Delta u(t-1), \ldots, \Delta u(t-m-1)]^T$. The initial matrix $P(0)$ is set arbitrarily. The online estimation of θ, i.e., $A(z^{-1})$ and $B(z^{-1})$, is hence used for the optimal control law $u^*(t)$ in (8) and (9).

The closed-loop stability analysis of the optimal control law (8) and (9) together with RLSE can be found in [19], [26], and [27]. To facilitate the effective application of the optimal control law for the ALD process, we summarize the procedure of selecting the controller parameters H_p, H_u, and λ in (6), μ in (11), and α in (7) as follows.

1) Discretize the offline identified transfer function $G(s)$ in (1) into $G_d(z^{-1}) = (z^{-d}A(z^{-1})/B(z^{-1}))$, and then obtain the unit step response series $\{g_1, g_2, \ldots, g_\infty\}$, where g_∞ is the steady-state output value of the step response.
2) Set the positive integer H_p moderately bigger than d.
3) Let $\hat{A}(z^{-1})$ and $\hat{B}(z^{-1})$ be the identification of $A(z^{-1})$ and $B(z^{-1})$ attained by the RLSE method (11), respectively. If $g_1 \geq g_\infty/2$ and both $G_d(z^{-1})$ and the unmodeled dynamics $(A(z^{-1})/B(z^{-1})/\widehat{A}(z^{-1})/\widehat{B}(z^{-1}))$ are Hurwitz, we set $H_u = H_p$; otherwise, $H_u = 1$.
4) Pick the weight λ according to the following conditions:

$$\sum_{i=1}^{H_p} g_i(g_{i+1} - g_i) \geq \lambda, \quad \sum_{i=1}^{H_p} g_i^2 + 2\lambda > \sum_{i=1}^{N} g_i(g_\infty - g_i). \tag{12}$$

5) Set the forgetting factor $\mu = 0.9$ and the softening factor $\alpha = 0.9$. According to step response simulations on $G(z^{-1})$, if the control signal is too aggressive (or the output oscillations/overshoots are too severe more than 2.0 °C), increase λ, α, and H_p or decrease μ.

It is shown in [26] that unmodeled dynamics are allowed and H_u can be greater than one, which allows an extra degree of freedom in the controller design. GPC's capability in dealing with unmodeled dynamics and external disturbances provides motivation for application in ALD process control. Accordingly, we have initialized the parameter values and tuned them according to the experimental control performance. The optimized parameters are set as $H_p = H_u = 15$, $\lambda = 0.7$, $\mu = 0.9$, and $\alpha = 0.98$.

In the present ALD process, input/output/state constraints are not considered as a major issue in practice. Therefore, the optimization problem (6) and the adopted GPC strategy do not incorporate the constraints. In case these constraints become notable, GPC also provides the capability to deal with input/output/state constraints [23], [25].

IV. Control Experiments With External Disturbances

There are three typical external disturbances that affect ALD processes: 1) pressure variation; 2) precursor pulse; and 3) sample loading perturbation. In this section, we aim to examine GPC performance in handling these disturbances.

A. GPC With Pressure Variation Disturbances

Throughout the four stages listed in Table I, the different pressures dictate that the chamber dynamics have four different models as well. Chamber pressure is influenced by variations in carrier inert gas flow rate and pumping state, which inevitably lead to deviations from equilibrium temperature. Under the pressure variation disturbances in Fig. 4(c), the evolutions of substrate temperature $y(t)$ and control voltage $u(t)$ are shown in Fig. 4(a) and (b), respectively. It is observed that chamber temperature recovers to the set point for the system that suffers step pressure variation disturbances during all four stages. With a variance from 10 to 80 Pa, the overshoot and settling time of $y(t)$ are 1.6 °C and 700 s, respectively. During the third stage, the overshoot and settling time of $y(t)$ change to 1.3 °C and 2000 s, respectively, and the nadir of the temperature reduction is 6.2 °C. Thus, both the feasibility and the robustness of the GPC-based control system are verified for pressure variation disturbances. It is worth noting

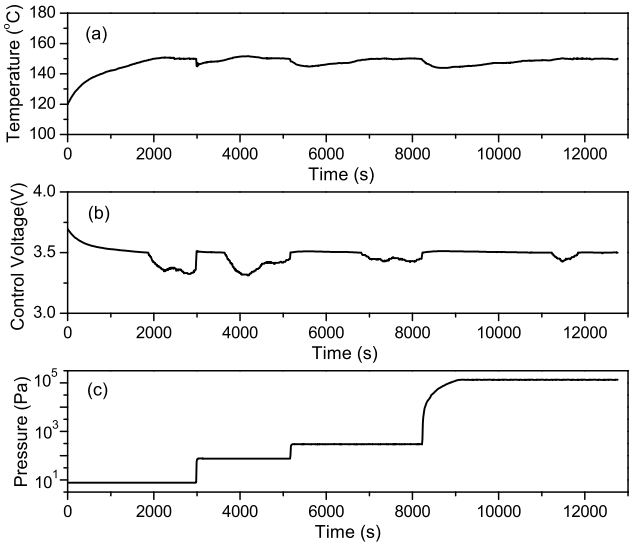

Fig. 4. (a) Temperature $y(t)$, (b) control voltage $u(t)$, and (c) chamber pressure under pressure variation disturbances.

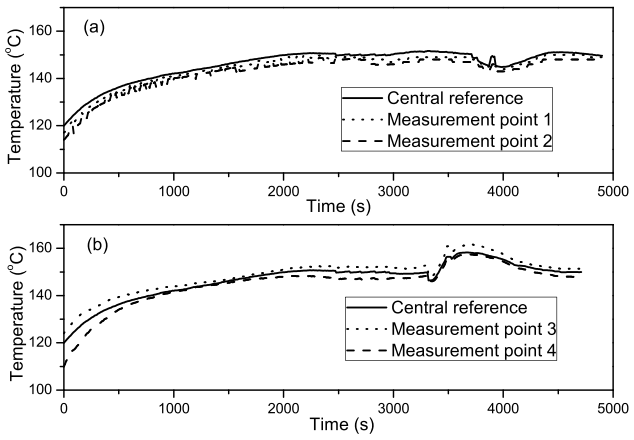

Fig. 5. Temperature evolvement of the measured points referencing to the central point. (a) Measured points near the inlet and outlet, respectively. (b) Measured points near the door.

that the maximum temperature overshoot is 2.0 °C, since larger overshoots will lead to thermal decomposition or other undesired side reactions.

Taking the steps toward achieving the goal of an evenly distributed temperature field on the ALD substrate, we carry out two experiments that measure temperature at four positions with different gas flows. The first experiment measures the temperature at point 1 near the gas inlet and at point 2 near the gas outlet. The second experiment measures temperature at point 3 near the sample loading door and at point 4 far away from the sample loading door, as shown in Fig. 1(a). It is observed in Fig. 5(a) and (b) that the measured temperature at each point in the chamber follows the central reference to reach equilibrium. Thus, the desired temperature is achieved evenly to facilitate the film growth.

B. GPC With Precursor Pulse Disturbances

During the ALD reaction, precursor vapor is pulsed into the chamber with inert carrier gas. The pulse time is short

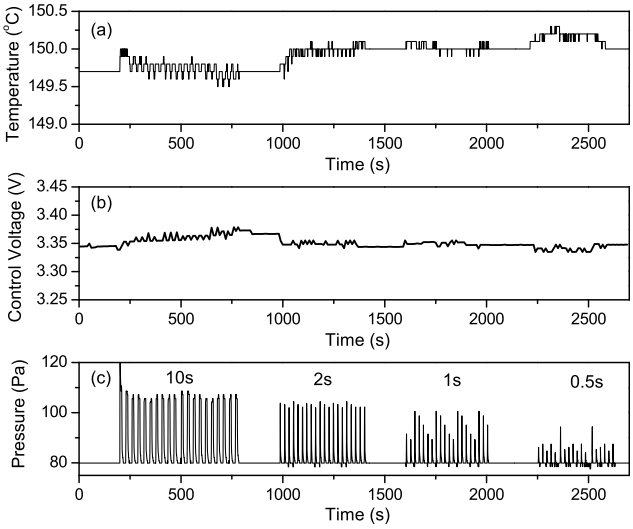

Fig. 6. (a) Temperature $y(t)$, (b) control voltage $u(t)$, and (c) precursor pressure under 10-, 2-, 0.5-, and 0.1-s precursor pulse disturbances, respectively.

when saturated with precursor of high vapor pressure, but long for low vapor pressure precursors or large deposition areas. To investigate the temperature response in the presence of precursor pulse disturbances, four precursor pulse times are in the ordering of 10 s, then 2 s, then 0.5 s, and then 0.1 s, which are selected for 20 cycles of repetitive pulsing, respectively. It is observed in Fig. 6 that all the four precursor pulses substantially disturb the equilibrium temperature at a base pressure of 80 Pa. Moreover, temperature $y(t)$ decreases more rapidly with increasing pressure pulse amplitude, and the oscillations in $y(t)$ decrease with declining pulse time. As shown in Fig. 6(a), there is a negligible difference between the temperature oscillations for 10- and 2-s pulses, since they have similar stepped pressure jumps with the saturated precursor vapor. In contrast, when the pulse times are 0.5 and 0.1 s, the pressure pulse amplitude decreases in Fig. 6(c). Hence, the maximum temperature variation is reduced to 0.3 °C, with variations less than 0.1 °C for the 0.1-s pulse in Fig. 6(a). Even with a small temperature reduction of 0.1 °C, the control voltage $u(t)$ calculated by the GPC law (8) serves to alleviate the temperature oscillations, as shown in Fig. 6(b). Note that the difference of Figs. 4 and 6 lies in that the pressure disturbances in Fig. 4 appear before the ALD reaction happens, while the precursor pulse disturbances in Fig. 6 appear during the ALD reaction. Therefore, medium temperature deviations are acceptable in Fig. 4, but not in Fig. 6 since even very small temperature variations may affect the thin-film quality, not to mention the high-frequency fluctuations. Therefore, the effectiveness and robustness of the developed GPC system are validated for precursor pulse disturbances.

C. GPC With Sample Loading Disturbances

To date, most ALD systems work in batch mode, in which the steady dynamics of the chamber temperature are inevitably perturbed by sample loading and unloading operations. For an industrial equipment, buffer chambers where samples are

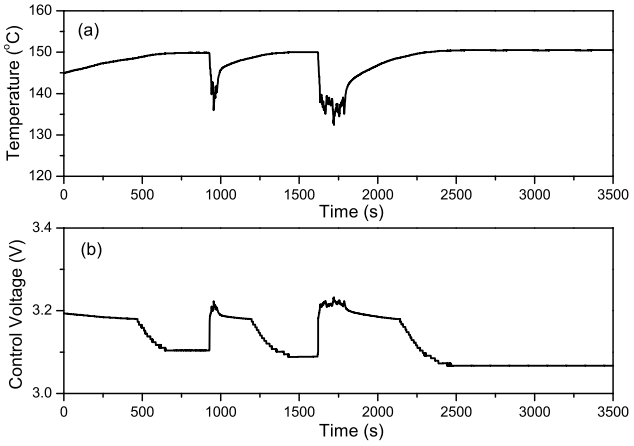

Fig. 7. (a) Temperature $y(t)$ and (b) control voltage $u(t)$ under sample loading disturbances.

transported by robotic arms under vacuum can accelerate the operation. For research-grade tools, however, the reactor discussed in this brief requires a long time to vent the system to atmospheric conditions, and changing the sample holder can be complicated. Accordingly, it is necessary to examine the temperature recovering efficiency and robustness of the developed GPC system in the presence of sample loading disturbances. Hereby, we conduct two experiments with disturbances that last for two different durations: 1 and 3 min. As shown in Fig. 7, the control voltage $u(t)$ sharply increases to prevent temperature reduction when the door is opened for sample loading/unloading. To alleviate the temperature overshoot and the input, one can increase the weight λ (6) or the softening factor α (7) when the temperature approaches the set point. Thus, the chamber temperature remains stable during sample loading and recovers quickly when the disturbance subsides. During 1 min of sample loading disturbance, the chamber temperature $y(t)$ decreases by 8 °C, and then recovers to the set point after 10 min. During 3 min of disturbance, temperature $y(t)$ sharply decreases by 15 °C, and recovers after 15 min, verifying the efficiency and robustness of GPC for sample loading/unloading operations. Hence, the robustness of GPC is desirable for guaranteeing the quality of deposited films, which is demonstrated in the following section.

V. Film Growth Experiments by ALD

The purpose of this brief is to improve the quality of deposited films by ALD. Thus, thin-film growth experiments are conducted using the GPC algorithm for comparison with open-loop control and PID control.

The deposition of Al_2O_3 thin films is performed by alternately dosing trimethyl aluminum (TMA) and deionized water (18.2 MΩ). Ultrahigh purity nitrogen (99.999%) gas is continuously flowed through the chamber at 100 sccm as the carrier and purging gas. The precursor pulse times of TMA and water are both 0.1 s. Meanwhile, an inert gas purge of 8 s is used between each precursor to avoid nonself-limiting growth. The base pressure while running the growth experiments is maintained at 80 Pa. Film thickness is measured

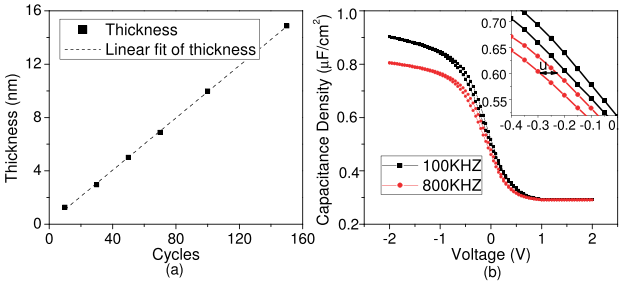

Fig. 8. (a) Growth per cycle and (b) C–V characteristic of Al_2O_3 film on silicon substrate.

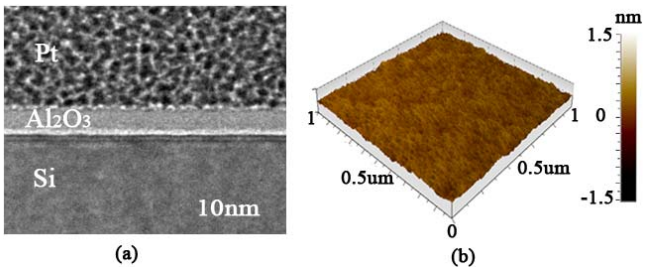

Fig. 9. (a) TEM images of Al_2O_3 thin film. (b) 3-D AFM images of Al_2O_3 thin film.

by spectroscopic ellipsometry (SE, J. A. Woolman M2000) and calibrated by transmission electron microscopy (TEM, Tecnai G2 F30). Linear growth is observed after 5 cycles with growth rate at 0.9 Å/cycle, as shown in Fig. 8(a). The cross-sectional TEM image of an Al_2O_3 thin film deposited for 50 cycles is smooth and homogenous [Fig. 9(a)]. The film thicknesses measured by SE and TEM match quite well, indicating a long-range film thickness uniformity. Atomic force microscopy (AFM, Agilent 5500) is performed in tapping mode to characterize the surface topography and roughness over an area of 1 um × 1 um. The height in the Z-direction indicates that the thin film surface is atomically flat with a root-mean-square (rms) surface roughness of 0.17 nm, as shown in Fig. 9(b). C–V measurements (Keithley 4200) are conducted to analyze the electrical properties of the Al_2O_3 film with sweeping frequencies of 100 and 800 kHz. The low hysteresis with 60 mV of the C–V curves between Al_2O_3 and SiO_2 substrate is similar to [28] and [29] [see Fig. 8(b)]. Furthermore, the calculated equivalent oxide thickness of Al_2O_3 stacked on 3.9-nm SiO_2 is approximately 4.17 nm, and the static dielectric constant K value of Al_2O_3 is 8.72, which is consistent with the range of 7–9 reported previously [30].

A. Efficiency Improvement

To show the superiority of GPC for the ALD process, GPC, PID, and open-loop controls are applied to the plant under the influence of a 3-min sample loading disturbance. For the open-loop control strategy, the constant control voltage is obtained by a table-seeking method, or searching the control voltage corresponding to the steady-state target temperature. By contrast, the three parameters of PID approach are initially obtained from the Siemens PLC self-tuning module. Afterward, they are tuned online according to the

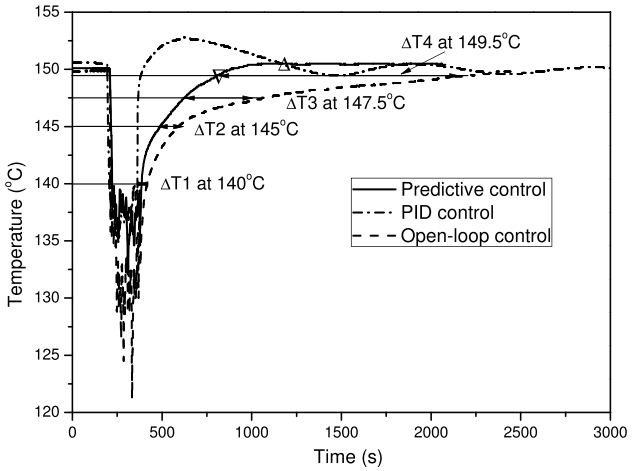

Fig. 10. Comparison of GPC, PID, and open-loop control. The setting times of GPC, open-loop, and PID approaches are 10, 33, and 21 min, respectively. Moreover, PID has an overshoot of 3 °C, which is unacceptable for ALD techniques.

TABLE II
THICKNESS AND SAVED SETTLING TIME

Initial temperature(°C)	Thickness (nm)	Settling time saved (min)	Efficiency
140	4.98±0.06	0.5	3%
145	5.01±0.04	2	12%
147.5	4.99±0.02	8	35%
149.5	4.96±0.02	23	61%

over shootings, settling times, tracking errors, and temperature oscillations of the simulations and experiments. As shown in Fig. 10, the temperature controlled by PID stabilizes at the △ marker, while GPC the ∇ marker. GPC stabilizes 5.8 min faster than the PID controller, and afterward, the temperature controlled by GPC settles in a range of 149.5 °C–150.5 °C. Hence, GPC has a remarkably shorter stabilization time than PID. In addition, PID has a larger overshoot, 3 °C, which is unacceptable since an overshoot may lead to decomposition of the precursor. Thus, GPC outperforms PID control in temperature recovering capability. Next, GPC is compared with open-loop control. Four temperatures are selected, {140 °C, 145 °C, 147.5 °C, and 149.5 °C}, as listed in Table II. The stabilization times by GPC are shorter than open-loop control by 0.5, 2, 8, and 23 min, respectively. This implies that the corresponding efficiencies are increased by 3%, 12%, 35%, and 61%, respectively. Therefore, during sample loading disturbances, the stabilization time of GPC is shorter than that of open-loop control, and the advantage is intensified as the temperature approaches the set point. To check the generality of the observation, growth experiments are conducted beginning from different initial temperatures, since Al_2O_3 is known to have a nearly constant growth rate in the target temperature range studied [1]. The thickness and uniformity of each thin film are listed in Table II. Though the bulk growth rate at each temperature is nearly constant, the uniformity of the film changes due to temperature ramping and variation. For example, once the temperatures stabilize at 147.5 °C and 149.5 °C, the point-to-point variations

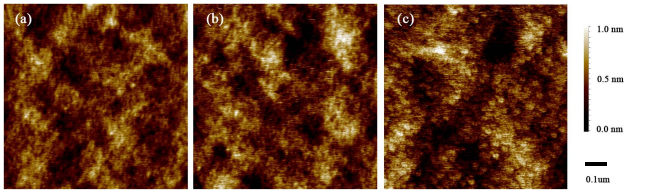

Fig. 11. 2-D AFM images of Al_2O_3 thin film with (a) GPC [$y(0) = 147.5$ °C], (b) open-loop control [$y(0) = 147.5$ °C], and (c) PID control [$y(0) = 150$ °C].

are approximately equivalent. For this experiment, $y(0) = 147.5$ °C is chosen to expedite the ALD process, and 8 min of deposition time is saved, which is equivalent to 35% of 50 cycles of ALD runs. More significantly, for other ALD reactions with tighter temperature windows, or when growth rate is temperature dependent, GPC's superiority is intensified since a more accurate temperature point can be achieved. Hence, the merits of GPC are verified.

B. Microscopic Morphology Improvement

The microscopic properties of thin film are evaluated to determine the effectiveness of the ALD chamber temperature controller. After deposition, although similar macroscopic uniformities are produced by GPC, PID, and open-loop control (0.02 nm for a 5-nm film), the microscopic morphology differences among the three control approaches can be clearly observed in Fig. 11. Therein, the rms roughness of the film deposited using the GPC algorithm is 0.17 nm, 0.46 nm for open-loop control, and 0.42 nm by PID control. This improvement is associated with the fact that GPC has a control voltage compensation feature for temperature variations caused by precursor pulse disturbances, which substantially attenuates temperature overshoot and oscillations during deposition. Consequently, temperature variation controlled by GPC remains within ±0.05 °C (as described in Section III), while that of open-loop control exceeds ±0.15 °C. Although the allowable temperature range for Al_2O_3 deposition is large, low temperature variations are desirable so as to guarantee microscopic uniformity. For narrower operating temperature ranges, GPC is more beneficial for achieving a constant temperature. In summary, GPC-controlled systems have been proven to be feasible and superior in experimental ALD processes.

VI. CONCLUSION

This brief establishes a closed-loop chamber temperature control system for ALD processes based on a GPC algorithm. This control system substantially accelerates the deposition procedure and, hence, improves the deposition uniformity of nanoscale-thickness thin films. The merits of the controller lie in the ability to quickly reach a target temperature range with small overshoot and oscillation in the presence of three typical external disturbances. Extensive experimental results verify that the grown films with GPC have better microscopic morphologies and uniformities than both PID and open-loop control due to the improved ability of withstanding external disturbances.

ACKNOWLEDGMENT

The authors would like to thank T. Zhou, Z. Deng, and C. Duan for designing and building the ALD reactor. The authors would also like to thank B. Huang, K. Tian, and X. Liu for assisting with ALD experiments.

REFERENCES

[1] S. M. George, "Atomic layer deposition: An overview," *Chem. Rev.*, vol. 110, no. 1, pp. 111–131, 2010.

[2] S. M. George, A. W. Ott, and J. W. Klaus, "Surface chemistry for atomic layer growth," *J. Phys. Chem.*, vol. 100, no. 31, pp. 13121–13131, 1996.

[3] O. Sneh, R. B. Clark-Phelps, A. R. Londergan, J. Winkler, and T. E. Seidel, "Thin film atomic layer deposition equipment for semiconductor processing," *Thin Solid Films*, vol. 402, nos. 1–2, pp. 248–261, 2002.

[4] X. Du and S. M. George, "Thickness dependence of sensor response for CO gas sensing by tin oxide films grown using atomic layer deposition," *Sens. Actuators B, Chem.*, vol. 135, no. 1, pp. 152–160, 2008.

[5] A. C. Dillon, A. W. Ott, J. D. Way, and S. M. George, "Surface chemistry of Al_2O_3 deposition using $Al(CH_3)_3$ and H_2O in a binary reaction sequence," *Surf. Sci.*, vol. 322, nos. 1–3, pp. 230–242, 1995.

[6] R. Chen, H. Kim, P. C. McIntyre, and S. F. Bent, "Self-assembled monolayer resist for atomic layer deposition of HfO_2 and ZrO_2 high-κ gate dielectrics," *Appl. Phys. Lett.*, vol. 84, no. 20, pp. 4017–4019, 2004.

[7] R. Chen and S. F. Bent, "Chemistry for positive pattern transfer using area-selective atomic layer deposition," *Adv. Mater.*, vol. 18, no. 8, pp. 1086–1090, 2006.

[8] A. W. Ott, J. W. Klaus, J. M. Johnson, and S. M. George, "Al_2O_3 thin film growth on Si(100) using binary reaction sequence chemistry," *Thin Solid Films*, vol. 292, no. 1, pp. 135–144, 1997.

[9] S. J. Qin and T. A. Badgwell, "A survey of industrial model predictive control technology," *Control Eng. Pract.*, vol. 11, no. 7, pp. 733–764, 2003.

[10] H. T. Zhang, M. Z. Q. Chen, and Z. Chen, "Nonlinear Laguerre–Volterra observer controller and its application to process control," *Int. J. Robust Nonlinear Control*, vol. 20, pp. 412–423, 2010.

[11] H.-T. Zhang, Z. Chen, Y. Wang, T. Qin, and M. Li, "Adaptive predictive control algorithm based on Laguerre functional model," *Int. J. Adapt. Control Signal Process*, vol. 20, no. 2, pp. 53–76, 2006.

[12] M. Alamir, N. Sheibat-Othman, and S. Othman, "Constrained nonlinear predictive control for maximizing production in polymerization processes," *IEEE Trans. Control Syst. Technol.*, vol. 15, no. 2, pp. 315–323, Mar. 2007.

[13] C. Vermillion, J. Sun, and K. Butts, "Predictive control allocation for a thermal management system based on an inner loop reference model—Design, analysis, and experimental results," *IEEE Trans. Control Syst. Technol.*, vol. 19, no. 4, pp. 772–781, Jul. 2011.

[14] P. Gil, J. Henriques, A. Cardoso, P. Carvalho, and A. Dourado, "Affine neural network-based predictive control applied to a distributed solar collector field," *IEEE Trans. Control Syst. Technol.*, vol. 22, no. 2, pp. 585–596, Mar. 2014.

[15] D. Q. Mayne, J. B. Rawlings, C. V. Rao, and P. O. M. Scokaert, "Constrained model predictive control: Stability and optimality," *Automatica*, vol. 36, no. 6, pp. 789–814, 2000.

[16] M. Alpbaz, H. Hapoğlu, and G. Özkan, "Experimental application of generalized predictive control of the temperature in a polystrene polymerization reactor," *Chem. Eng. Commun.*, vol. 191, no. 9, pp. 1173–1184, 2004.

[17] E. Katende and A. Jutan, "Experimental evaluation of predictive temperature control for a batch reactor system," *IEEE Trans. Control Syst. Technol.*, vol. 8, no. 1, pp. 2–13, Jan. 2000.

[18] W. He, B. Chu, R. Gu, H. Zhang, B. Shan, and R. Chen, "The application of generalized predictive control in the radiant heating atomic layer deposition reactor," in *Proc. IEEE Int. Symp. Assembly Manuf. (ISAM)*, Xi'an, China, Jul./Aug. 2013, pp. 37–40.

[19] D. W. Clarke, C. Mohtadi, and P. S. Tuffs, "Generalized predictive control—Part I. The basic algorithm," *Automatica*, vol. 23, no. 2, pp. 138–148, 1987.

[20] D. W. Clarke, C. Mohtadi, and P. S. Tuffs, "Generalized predictive control—Part II. Extensions and interpretations," *Automatica*, vol. 23, no. 2, pp. 149–160, 1987.

[21] Y. K. Ho, F. S. Mjalli, and H. K. Yeoh, "Generalized predictive control with dual adaptation," *Chem. Eng. Sci.*, vol. 84, pp. 479–493, Dec. 2012.

[22] M. F. Modest, *Radiative Heat Transfer*, 3rd ed. Amsterdam, The Netherlands: Elsevier, 2013.

[23] E. F. Camacho, "Constrained generalized predictive control," *IEEE Trans. Autom. Control*, vol. 38, no. 2, pp. 327–332, Feb. 1993.

[24] E. F. Camacho and C. Bordons, *Model Predictive Control*, 2nd ed. London, U.K.: Springer-Verlag, 2013.

[25] J. M. Maciejowski, *Predictive Control With Constraints*. Upper Saddle River, NJ, USA: Prentice-Hall, 2002.

[26] D. W. Clarke and C. Mohtadi, "Properties of generalized predictive control," *Automatica*, vol. 25, no. 6, pp. 859–875, 1989.

[27] H. W. Gomma, "Stability analysis for generalized predictive control (GPC) with different classes of uncertain systems," in *Proc. IEEE Int. Conf. Control Appl.*, Munich, Germany, Oct. 2006, pp. 984–989.

[28] H. Liu and P. D. Ye, "MoS_2 dual-gate MOSFET with atomic-layer-deposited Al_2O_3 as top-gate dielectric," *IEEE Electron Device Lett.*, vol. 33, no. 4, pp. 546–550, Apr. 2012.

[29] P. Ye, Y. Xuan, and H. C. Lin, "Capacitance-voltage characterization of atomic-layer-deposited Al_2O_3/InGaAs and Al_2O_3/GaAs metal-oxide-semiconductor structures," *ECS Trans.*, vol. 3, no. 3, pp. 59–69, 2006.

[30] J. Robertson, "High dielectric constant oxides," *Eur. Phys. J. Appl. Phys.*, vol. 28, pp. 265–291, Dec. 2004.